ACS OMEGA

Open Access

http://pubs.acs.org/journal/acsodf

Article

Selective Formation of Cu Active Sites with Different Coordination States on Pseudospinel $CuAl_2O_4$ and Their NO Reduction Catalysis

Aoi Okuda,* Taniyuki Furuyama, Toshiaki Sakai, Masato Machida, and Hiroshi Yoshida*

Cite This: *ACS Omega* 2024, 9, 11950−11957

Read Online

ACCESS | Metrics & More | Article Recommendations | Supporting Information

ABSTRACT: In the spinel framework, copper (Cu) in two distinct coordination states exhibits catalytic activity for NO reduction through different mechanisms. However, detailed exploration of their respective catalytic properties, such as the redox behavior of Cu and substrate molecule adsorption, has been challenging due to difficulties in their separate formation. In this study, we present the controlled formation of pseudospinel $CuAl_2O_4$, containing exclusively tetrahedrally or octahedrally coordinated Cu, achieved by manipulating aging temperature and O_2 concentration. Through these materials, we observed that in the CO−NO reaction, the step primarily determining the rate differs: NO reduction dominates with octahedrally coordinated Cu, whereas carbon monoxide (CO) oxidation is prominent with tetrahedrally coordinated Cu. The lower coordination number of Cu significantly benefits NO reduction but negatively impacts the CO−NO reaction, albeit positively influencing NO reduction in three-way catalytic reactions.

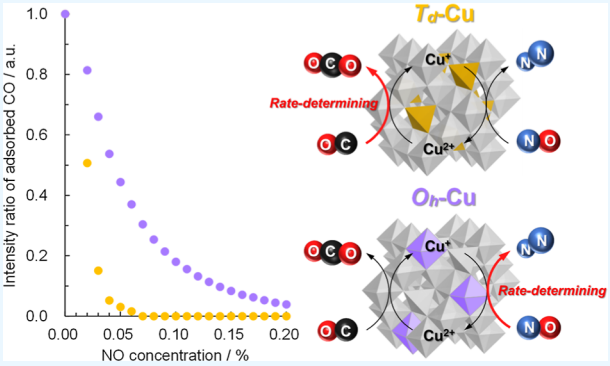

INTRODUCTION

Reducing pollutants remains a critical, ongoing challenge in activities producing harmful substances. In the realm of mobile applications, three-way catalysts (TWCs) have played a pivotal role in curbing pollutant emissions from gasoline-powered vehicles.[1−5] While platinum group metal (PGM) nanoparticles have been widely used in TWCs, their adoption has been restricted due to their high cost and limited availability. Hence, the pursuit of alternative catalytic materials, leveraging cost-effective and abundant transition metals, has garnered significant interest.[6−10] Investigations into various metals' efficacy, including Cu,[11−18] Ni,[19−21] and Co[22−24] have been conducted.

Automobile exhaust gas predominantly comprises nitrogen oxides (NO_x), carbon monoxide (CO), and unburned hydrocarbons like C_3H_6. Among these components, NO_x should be reduced while the other two components are necessary to oxide. While oxidation demands a stoichiometric or excess amount of O_2, its presence severely inhibits the NO_x reduction process. Additionally, developing catalysts for practical use in automotive emission control systems faces the challenge of thermal durability.[18,25−28] Exposure to gasoline engine exhaust at temperatures exceeding 800 °C for prolonged periods leads to severe thermal aging, causing significant sintering of supported metal nanoparticles or changes in the crystal structure, thus degrading the catalyst. To tackle these issues, investigations into solid solution catalyst effectiveness rather than supported metal structures have been explored.[16−18,27,29−32]

Incorporating Cu into a support material boosts the NO_x reduction activity by regulating the redox cycle through the movement of adjacent oxygen atoms. Additionally, this catalyst exhibits remarkable thermal stability, avoiding sintering from thermal degradation. Recent findings reported that Cu, when integrated into the tetrahedral site of γ-Al_2O_3 (T_d-Cu^{2+}), showed heightened catalytic performance in the NO−CO−C_3H_6−O_2 reaction, particularly in NO reduction.[18] This occurred due to thermal aging at high temperatures, which prompted Cu^{2+} incorporation into tetrahedral sites (T_d-Cu^{2+}) rather than octahedral ones (O_h-Cu^{2+}).[33,34] This T_d-Cu exhibited superior redox cycling, transitioning between T_d-Cu^{2+} and T_d-Cu^{+} via CO oxidation and NO reduction, consequently enhancing NO reduction in the three-way catalytic reaction. Enhancing activity further could be achieved by increasing the Cu occupancy within tetrahedral sites on spinel γ-Al_2O_3, but there are no existing reports on composite materials solely comprising T_d-Cu. As Areán and Vinuela reported, site occupancies of T_d-Cu^{2+}, O_h-Cu^{2+}, T_d-Al^{3+}, and O_h-Al^{3+} in a spinel $CuAl_2O_4$ are 0.649, 0.351, 0.351, and 1.649, respectively, indicating that surpassing a 65% Cu occupancy

Received: December 5, 2023
Revised: February 14, 2024
Accepted: February 21, 2024
Published: March 4, 2024

ratio in the most stable $CuAl_2O_4$ is thermodynamically challenging.[35] Therefore, developing a catalyst preparation technique to achieve high Cu occupancy within tetrahedral sites is crucial not only for enhancing the three-way catalytic activity but also for deepening our understanding of the relationship between catalytic properties and surface Cu coordination states.

In this study, our focus was on understanding how various reaction conditions—such as temperature, atmosphere, and aging time—affect the fine structure and coordination state when Cu species are incorporated into the framework of γ-Al_2O_3 through thermal aging. Our aim was to identify suitable preparation conditions to intentionally form T_d-Cu on spinel γ-Al_2O_3. To delve into the detailed structures of the Cu active sites and crystal structure, we employed techniques like X-ray diffraction (XRD), X-ray photoelectron spectroscopy (XPS), and diffuse reflectance ultraviolet, visible, and near-infrared spectroscopy (UV−vis−NIR). Additionally, we explored the catalytic activity of both T_d-Cu and O_h-Cu in a three-way catalytic reaction. We specifically investigated their NO reduction properties through kinetic analysis and by observing adsorbed species using in situ Fourier transform infrared (FT-IR) spectroscopy techniques.

MATERIALS AND METHODS

Preparation and Characterization. An Al_2O_3-supported 6 wt % Cu catalyst (Cu/Al_2O_3) was prepared by conventional impregnation using aqueous $Cu(NO_3)_2$ solutions (99.0% purity, Wako Pure Chemical Industries, Ltd.) and commercially available γ-Al_2O_3 (99.99% purity, 159 $m^2\ g^{-1}$, AKP-G15, provided by the Catalysis Society of Japan). The impregnated samples underwent overnight drying at 110 °C. Subsequently, the sample was thermally treated at 600 °C for 3 h in a gas mixture stream of a mixture of O_2 and N_2 with varying O_2 concentrations (0, 50, and 100%). Further thermal aging occurred at 900 or 1000 °C for 2−25 h in the same gas stream.

The crystal structure of the sample was determined by powder XRD (MiniFlex600, Rigaku) using monochromatic Cu Kα radiation (λ = 1.54 Å). The Brunauer−Emmet−Teller surface area (S_{BET}) was calculated by using N_2 adsorption isotherms measured at −196 °C (BELSORPmaxII, MicrotracBEL, Inc.). The oxidation states and surface concentrations of Cu were determined by XPS using monochromatic Al Kα radiation (12 keV, K-Alpha, Thermo Fisher Scientific), and the binding energies were charge-referenced to C 1s at 285 eV. We used XPS as a nondestructive analysis to measure the surface Cu concentration instead of general N_2O chemisorption, namely, the absolute surface Cu concentration was defined by assigning the relative surface Cu concentration calculated from XPS to the S_{BET} value. The coordination state of Cu on γ-Al_2O_3 was confirmed by using a UV−vis−NIR spectrometer (V-570, JASCO Co.) and a diffuse reflectance cell. The obtained spectra were treated according to the Kubelka−Munk theory.

Catalytic Reactions. The catalytic NO−CO−C_3H_6−O_2−H_2O reaction was performed in a continuous fixed-bed reactor at atmospheric pressure. The catalyst (0.1 g, 20 mech) was placed in a quartz tube (inside diameter of 4 mm) using quartz wool. The activity assessment involved heating the catalyst bed from room temperature to 600 °C at a rate of 10 °C min^{-1} while supplying a simulated gas mixture (0.05% NO, 0.50% CO, 0.04% C_3H_6, 0.40% O_2, 10% H_2O, and N_2 balance, 100 $cm^3\ min^{-1}$) at atmospheric pressure. The gas composition corresponded to a stoichiometric air-to-fuel ratio (A/F) of 14.6 based on weight, where all gases can be completely converted into a mixture of CO_2, H_2O, and/or N_2. The effluent gas underwent analysis using nondispersive infrared N_2O/CO/C_3H_6 (VA-5000, HORIBA) and a chemiluminescence detection NO gas analyzer (NOA-7100, SHIMADZU).

The effects of the CO/NO partial pressure on the CO−NO reaction rate were determined at 240 °C, maintaining steady-state conversions below 20% in a differential reactor. The CO partial pressure varied from 0.1 to 0.2 kPa while maintaining a constant NO partial pressure of 0.2 kPa. The NO partial pressure varied from 0.1 to 0.2 kPa while the CO partial pressure was kept constant at 0.2 kPa.

In Situ FT-IR Measurement. The influence of the Cu coordination state on molecular adsorption was systematically investigated by using FT-IR techniques. In situ FT-IR spectra of CO adsorbed on Cu/Al_2O_3 samples with different Cu coordination states were obtained using an FT-IR spectrometer (FT/IR-4X, JASCO Co.) with a temperature-controlled diffuse reflectance reaction cell and a mercury−cadmium−telluride detector. The sample underwent grinding and was then placed in the cell to form a flat surface. The cell was heated to 200 °C at a constant rate of 10 °C min^{-1} and held at this temperature for 15 min under a supply of N_2. After the mixture was cooled to 50 °C, the background spectrum was collected. The sample was exposed to a gas stream containing 5% CO balanced with N_2 to reduce Cu^{2+} to Cu^+ at different temperatures depending on the sample. The CO reduction temperature for each sample was determined from the CO temperature-programmed reduction (CO-TPR) results (Figure S1) prior to the measurements. After removal of gaseous CO by a N_2 flow at the same temperature, the sample was cooled to 50 °C.

We first determined the CO temperature-programmed desorption to compare the strength of CO adsorption on Cu^+ with different coordination states. After exposure to a 5% CO stream for 30 min, gaseous CO was removed with N_2 for 15 min, and the FT-IR spectrum was collected. The temperature was then increased in 10 °C increments, and the spectra were collected at each temperature, and the decrease in the absorption band of CO adsorption with increasing temperature was discussed. The influence of the copresence of NO in the CO adsorption was also evaluated. After pretreatment, the sample was exposed to a stream of 0.2% CO for 30 min and the spectrum was collected in the absence of NO. The NO concentration was then increased in 0.01% increments from 0 to 0.2%, and the spectra were collected under each condition. Their relative intensities to those in the absence of NO were compared.

RESULTS AND DISCUSSION

Structure Change of Supported Cu with High-Temperature Treatment under Different Atmospheres. The presence of Cu deposited on Al_2O_3 as CuO particles below 700 °C is well-documented, while exposure to higher thermal environments triggers a reaction between CuO and the Al_2O_3 support, resulting in the formation of pseudospinel $CuAl_2O_4$.[18] Figure 1 shows the XRD patterns of Cu/Al_2O_3 following a brief 2 h thermal aging under different atmospheres. None of the samples exhibited diffraction peaks characteristic of crystalline CuO, signifying the immediate integration of supported Cu^{2+} ions into the γ-Al_2O_3 framework

https://doi.org/10.1021/acsomega.3c09704
ACS Omega 2024, 9, 11950−11957

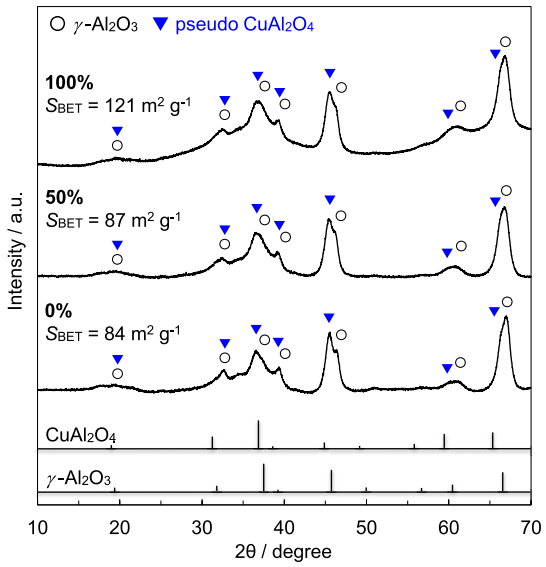

Figure 1. XRD patterns of Cu/Al_2O_3 samples after thermal aging at 900 °C for 2 h under different O_2 concentrations (0, 50, and 100%).

during the first stage of thermal aging, irrespective of the atmosphere's O_2 concentration.[18,27,36−38]

The presence of diffraction peaks corresponding to spinel-structured $CuAl_2O_4$, alongside those of γ-Al_2O_3, further corroborated the formation of pseudospinel $CuAl_2O_4$ on the outermost surface of γ-Al_2O_3. Notably, despite sharing the same crystal structure, different specific surface areas (S_{BET}) were observed, contingent upon the concentration of the O_2 in the atmosphere. Samples treated in 0 and 50% O_2 experienced a decline in S_{BET} to 84−87 $m^2\ g^{-1}$ due to thermal sintering. Conversely, the sample treated in 100% O_2 exhibited the highest value of 126 $m^2\ g^{-1}$, suggesting the potential suppression of thermal sintering in Cu/Al_2O_3 within high-temperature environments featuring elevated O_2 concentrations.

The detailed structure of the Cu sites incorporated in γ-Al_2O_3 was determined through diffuse reflectance UV−vis−NIR measurements (Figure 2). Two absorption bands, ranging

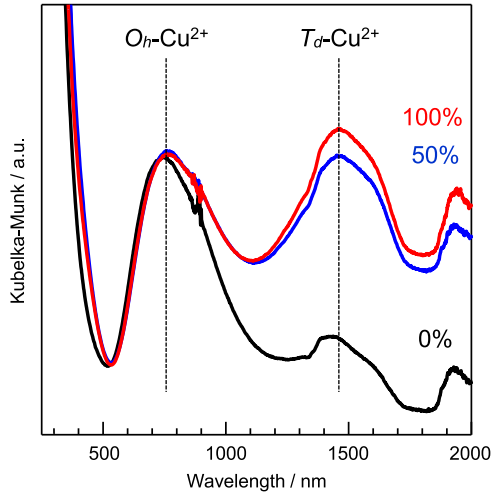

Figure 2. Diffuse reflectance UV−vis−NIR spectra of Cu/Al_2O_3 after thermal aging at 900 °C for 2 h under different O_2 concentrations (0, 50, and 100%).

from 400 to 800 nm and 1000 to 1700 nm, were attributed to the d−d transitions in octahedrally (O_h-Cu^{2+}) and tetrahedrally (T_d-Cu^{2+}) coordinated Cu^{2+}, respectively.[18,30,39,40] Upon thermal aging without O_2, the intensity peak of O_h-Cu^{2+} at 750 nm significantly exceeded that of T_d-Cu^{2+} at 1500 nm. This indicated a predominant occupation of octahedral sites (O_h-Cu^{2+}) within the spinel structure rather than tetrahedral sites (T_d-Cu^{2+}). Conversely, spectra from the samples aged under 50 and 100% O_2 concentration revealed a marked enhancement in the T_d-Cu^{2+} band at 1500 nm. This shift indicated that thermal aging at high O_2 concentrations prompted the incorporation of Cu^{2+} ions into tetrahedral sites, a phenomenon not previously reported. Thermodynamically, this occurrence aligns with the phase diagram of the Cu−Cu_2O−CuO system. At temperatures above 900 °C and under low O_2 concentrations, Cu_2O predominates due to the thermal decomposition of CuO. Consequently, thermal aging induces the formation of a solid solution between Cu_2O and γ-Al_2O_3, leading to monovalent Cu^+ occupying octahedral sites (O_h-Cu^+). Conversely, under high O_2 concentrations (50 and 100%), CuO stabilization hinders the thermal decomposition of CuO to Cu_2O. This condition fosters the formation of a solid solution between CuO and γ-Al_2O_3, resulting in divalent Cu^{2+} (T_d-Cu^{2+}) occupying both tetrahedral and octahedral sites (O_h-Cu).

After prolonged thermal aging (25 h), the structural changes in Cu/Al_2O_3 were found to be significantly influenced by the difference in O_2 concentration, as shown in Figure 3. When

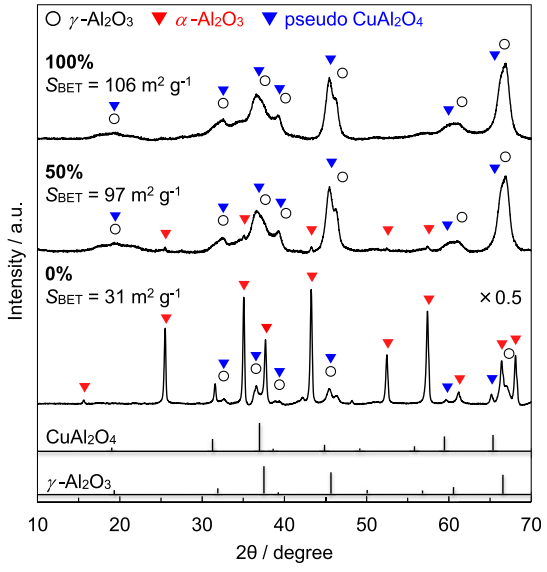

Figure 3. XRD patterns of Cu/Al_2O_3 after thermal aging at 900 °C for 25 h under different O_2 concentrations (0, 50, and 100%).

subjected to thermal aging without O_2, the sample exhibited the presence of highly crystalline α-Al_2O_3 and $CuAl_2O_4$, leading to a notable decrease in S_{BET} from 84 $m^2\ g^{-1}$ (2 h) to 31 $m^2\ g^{-1}$ (25 h). However, under conditions of high O_2 concentrations, such crystallization was unlikely, and XRD patterns akin to those observed in samples aged for a shorter duration (2 h) (Figure 1) were obtained, accompanied by higher S_{BET} values. For the sample aged under 50% O_2 concentration, minor diffraction peaks attributed to α-Al_2O_3 were noted. Interestingly, no such peaks were evident in the sample aged under 100% O_2, indicating that not only

https://doi.org/10.1021/acsomega.3c09704
ACS Omega 2024, 9, 11950−11957

crystallization but also the phase transition from γ-Al_2O_3 to α-Al_2O_3 can be suppressed under elevated O_2 concentrations during thermal aging.

The coordination states of the Cu active sites were assessed by using the UV−vis−NIR technique (Figure 4). Post-thermal aging in the absence of O_2, O_h-Cu^{2+} dominated the sample. However, under high O_2 concentrations, the spectra of the thermally aged Cu/Al_2O_3 strongly suggested larger T_d-Cu^{2+} sites compared to those of O_h-Cu^{2+} sites. Moreover, longer thermal aging notably amplified the relative intensities of T_d-Cu^{2+} at around 1500 nm. These findings indicate that the coordination state of Cu integrated into the γ-Al_2O_3 surface can be deliberately modified by regulating the O_2 concentration during thermal aging.

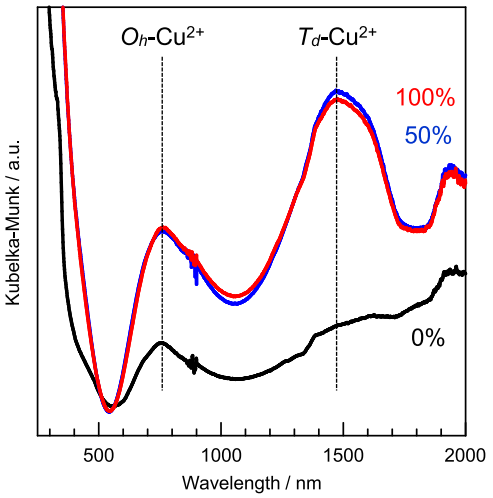

Figure 4. Diffuse reflectance UV−vis−NIR spectra of Cu/Al_2O_3 after thermal aging at 900 °C for 25 h under different O_2 concentrations (0, 50, and 100%).

Catalytic Properties of Cu Active Sites with Different Coordination States on the Al_2O_3 Surface. After prolonged thermal aging, we proceeded to assess the catalytic activities of the samples in the stoichiometric NO−CO−C_3H_6−O_2−H_2O reaction. Figure 5 shows the light-off curves for NO, CO, and C_3H_6 conversions over Cu/Al_2O_3 samples, each featuring Cu active sites with varied coordination states contingent upon the thermal aging atmosphere, as demonstrated in Figure 4. While the light-off curves for CO conversion remained consistent across all samples, catalysts hosting T_d-Cu sites exhibited higher activities in C_3H_6 oxidation and NO reduction. The peak appearance of the NO conversion at around 380 °C can be attributed to the selective catalytic reduction of NO in the presence of hydrocarbon over a Cu catalyst.[18,27,36,39,41,42] Chen et al. demonstrated that the NO reduction in the presence of C_3H_6 over 10 wt % Cu/Al_2O_3 at 350 °C decreased with further increase in temperature, and they concluded that the complete oxidation of C_3H_6 with excess O_2 at higher temperatures decreased the NO reduction.[41] Since similar reaction trends were obtained in Figure 5, we concluded that the peak appearance of NO conversion at around 380 °C is due to the selective catalytic reduction of NO by C_3H_6. Notably, the catalyst subjected to thermal aging under 100% O_2 concentration demonstrated the highest NO conversion rate of 73% at 600 °C. This superior activity can potentially be attributed to the structural disparity in Cu, specifically the prevalence of T_d-Cu, indicating its pivotal role in the three-way catalytic activity. Another contributing factor could be the abundance of Cu active sites. However, this latter hypothesis seems less plausible, as both catalysts subjected to high O_2 concentrations exhibited identical UV−vis−NIR spectra (Figure 4). To delve into this aspect further, we quantified the surface Cu concentration through XPS analysis and computed the specific surface area of Cu per weight using the S_{BET} value (Figure S2). Our analysis revealed a slightly higher specific surface area of Cu in the catalyst subjected to thermal aging under 100% O_2 concentration compared to that aged under 50% O_2 concentration, which likely contributes to its heightened NO reduction activity.

The aforementioned findings uncover two significant revelations. First, the thermal aging of Cu/Al_2O_3 under high O_2 concentrations impedes phase transition and/or crystallization processes. Second, there is a discernible selective formation of Cu active sites, exhibiting distinct coordination states on γ-Al_2O_3, achieved by precise control over the O_2

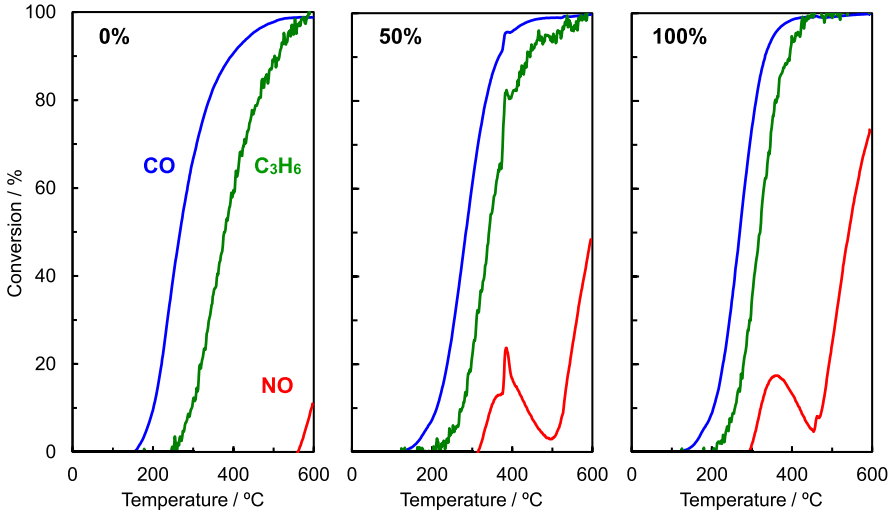

Figure 5. Light-off curves for a stoichiometric NO−CO−C_3H_6−O_2−H_2O reaction over Cu/Al_2O_3 after thermal aging at 900 °C for 25 h under different O_2 concentrations (0, 50, and 100%).

https://doi.org/10.1021/acsomega.3c09704
ACS Omega 2024, 9, 11950−11957

concentration. Particularly noteworthy is the selective formation of T_d-Cu, a state typically less favored concerning crystal field stabilization energy, which holds promise in unraveling the correlation between the coordination state of Cu and catalytic activity.

Given the observed augmentation in the relative intensity of UV−vis−NIR spectra corresponding to T_d-Cu with prolonged aging time (Figures 2 and 4), we subjected Cu/Al_2O_3 to harsher conditions to transform all of the Cu sites into the T_d-Cu state. Figure 6 shows the UV−vis−NIR spectra of Cu/Al_2O_3 after thermal aging at 1000 °C for 25 h under a 100% O_2 concentration. XRD analyses confirmed the emergence of highly crystalline $CuAl_2O_4$ and α-Al_2O_3 following thermal aging, concomitant with a decrease in the specific surface area to 8 m^2 g^{-1} (Figure S3). The sample showed low catalytic activity in the stoichiometric NO−CO−C_3H_6−O_2−H_2O reaction due to the drastic decrease in the specific surface area (Figure S4). Intriguingly, the presence of the band attributed to O_h-Cu^{2+} at 750 nm was absent, while the absorption band at 1500 nm, indicative of T_d-Cu, emerged prominently with high intensity. This outcome signifies the successful synthesis of Cu/Al_2O_3 wherein all Cu is incorporated solely into the tetrahedral sites (T_d-Cu) through thermal aging at 1000 °C under 100% O_2 conditions.

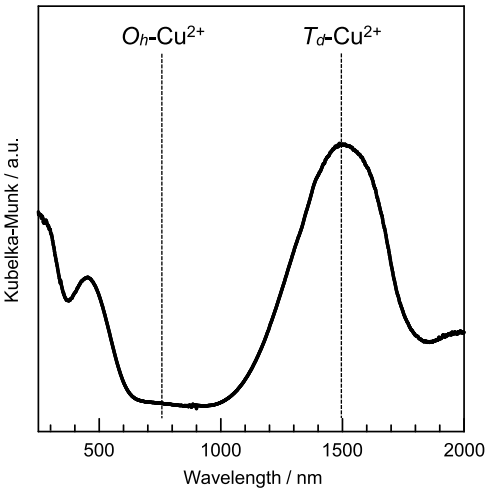

Figure 6. Diffuse reflectance UV−vis−NIR spectra of Cu/Al_2O_3 after thermal aging at 1000 °C for 25 h under 100% O_2 concentration.

To discern the catalytic characteristics of T_d-Cu and O_h-Cu active sites in NO reduction, we examined the dependence of the CO and NO partial pressure within the CO−NO reaction using Al_2O_3-supported Cu catalysts featuring either T_d-Cu or O_h-Cu sites. Model catalysts, namely, the Cu/Al_2O_3 after thermal aging at 900 °C for 25 h without O_2 (Figure 2) and after aging at 1000 °C for 25 h under 100% O_2 conditions (Figure 6), were utilized, referred to henceforth as the O_h-Cu sample and T_d-Cu sample, respectively.

The investigation involved determining the partial reaction orders concerning CO and NO at 240 °C based on the steady-state reaction rate in varying streams of CO and NO with different partial pressures (Figure 7). The observed positive dependencies on CO and NO suggest that the pivotal step in the reaction involves chemisorbed CO and NO molecules on the catalyst surface.

For the O_h-Cu sample, the reaction orders pertaining to CO and NO were found to be 0.34 and 0.52, respectively. These

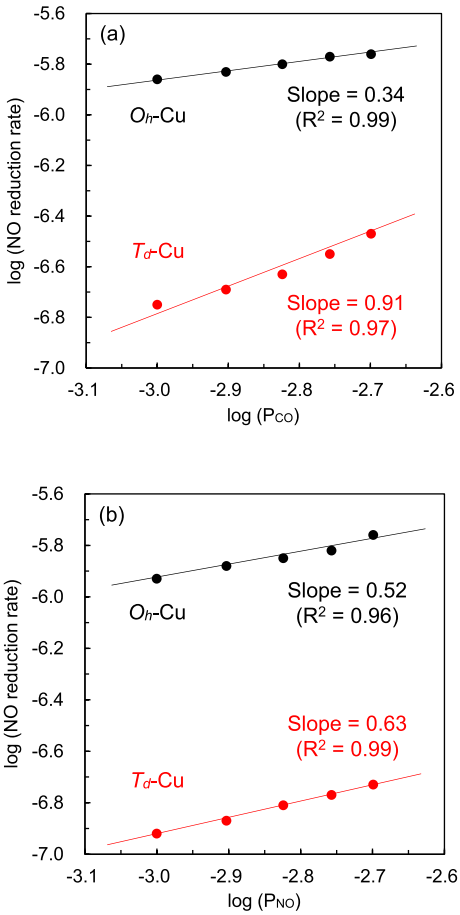

Figure 7. Dependence of the NO reduction rate and reaction order on (a) CO and (b) NO partial pressure in the CO−NO reaction over T_d-Cu and O_h-Cu samples at 240 °C.

values indicate a relatively higher dependence of the NO reduction rate on the NO concentrations. In contrast, the T_d-Cu sample exhibited a reaction order of 0.91 concerning CO (Figure 7a), significantly surpassing the NO reaction order of 0.63 (Figure 7b).

These findings strongly imply that the rate-determining step governing NO reduction over Cu active sites varies contingent upon the coordination states of Cu. Specifically, it appears that NO adsorption, crucial for the reoxidation of Cu^+ to Cu^{2+}, governs the rate-determining step over the O_h-Cu sites. Conversely, for T_d-Cu sites, the rate-determining step seems to involve CO adsorption, critical for the reduction of Cu^{2+} to Cu^+, as depicted in Figure 8. This distinction elucidates a significant mechanistic divergence in the NO reduction pathway over Cu active sites contingent upon their specific coordination states, delineating the distinct roles of O_h-Cu and T_d-Cu in catalyzing this reaction.

After kinetic analysis was conducted, it was discerned that the rate-determining step in NO reduction differs between T_d-Cu and O_h-Cu. To delve deeper into their catalytic properties, we systematically investigated the adsorption behavior of substrate molecules on Cu with varying coordination states. Initially, we compared the strength of the adsorption of CO on T_d-Cu and O_h-Cu using in situ diffuse reflectance infrared Fourier transform (DRIFT) measurements. The absorption bands associated with linearly adsorbed CO appeared consistently at a wavenumber of 2093 cm^{-1}, irrespective of

https://doi.org/10.1021/acsomega.3c09704
ACS Omega 2024, 9, 11950−11957

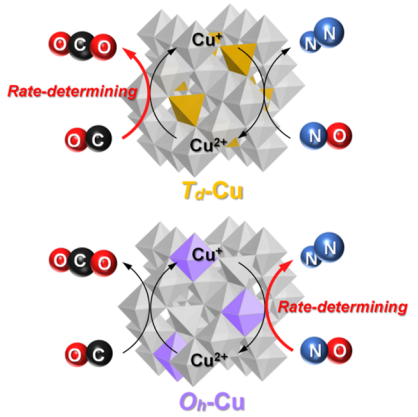

Figure 8. Different rate-determining steps of the CO−NO reaction over T_d-Cu and O_h-Cu sites by redox cycling of Cu.

the Cu coordination state, and those bands can be assigned to the CO adsorbed on the monovalent Cu^+.[32,43−45] The consistency of the wavenumbers of adsorbed CO implies that the electron back-donation from T_d-Cu^+ and O_h-Cu^+ to the π orbitals of CO is comparable, indicating that the influence of the Cu coordination state on the interaction between the CO molecules and surface Cu^+ is not significant. Moreover, the peak intensity demonstrated a gradual decrease with a rise in temperature (Figure S5). This consistent trend in the extent of peak intensity reduction with temperature suggests that there exists no significant disparity in the strength of CO adsorption between T_d-Cu and O_h-Cu.

We proceeded to assess the strength of the CO adsorption on Cu sites in the presence of NO. Figure 9a exhibits the DRIFT spectra detailing CO adsorption on T_d-Cu while incrementally introducing coexisting NO. In a parallel manner, the spectra depicting CO adsorption on O_h-Cu under the same conditions were also acquired (Figure 9b). To facilitate a comparison, the alteration in their relative intensities was plotted (Figure 9c). The diminishing peak intensity of CO adsorption in the presence of NO suggests competitive adsorption between CO and NO on Cu sites within the CO−NO gas mixture. Notably, the steeper decline in the CO adsorption peak intensity on T_d-Cu with rising NO concentration indicates a more pronounced inhibition of CO adsorption compared to O_h-Cu. Consequently, this effect contributes to a rate-limiting step involving the oxidation of Cu^{2+} to Cu^+ during the CO oxidation. Prior research has reported that a decrease in the coordination number of Cu^+ correlates with an increased adsorption energy of NO molecules, aligning with our current findings.[46,47] Hence, the lower coordination number characteristic of T_d-Cu confers a substantial advantage for NO adsorption over that of O_h-Cu. However, this unique property may exhibit a dual impact: while favoring NO reduction in the three-way catalytic reaction (Figure 5), it could potentially hinder CO−NO reactions due to the preferential adsorption of NO, inhibiting CO adsorption. This distinct attribute of T_d-Cu, particularly its robust NO adsorption capability, holds promise for the development of PGM-free deNO$_x$ catalysts. We anticipate uncovering novel catalytic functions inherent in a Cu catalyst primarily composed of T_d-Cu in the near future.

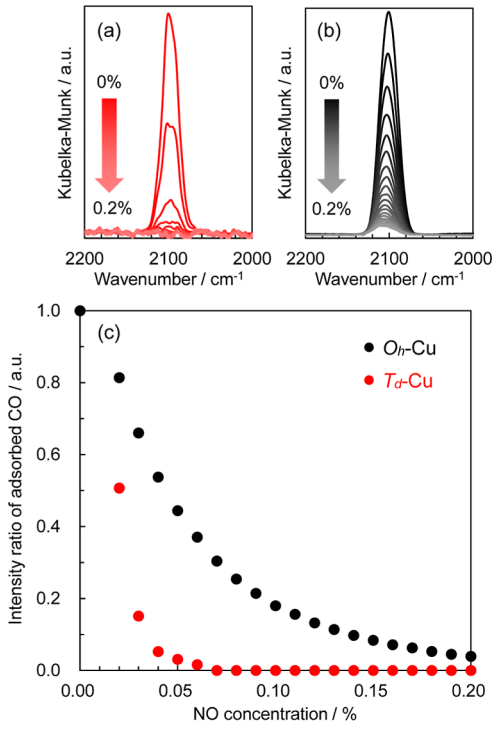

Figure 9. In situ DRIFT spectra of CO chemisorbed on (a) T_d-Cu^+ and (b) O_h-Cu^+ sites in the presence of NO at different concentrations. (c) Relative intensity of CO adsorption as a function of NO concentration.

CONCLUSIONS

The investigation focused on the formation process of pseudospinel $CuAl_2O_4$ on the surface of γ-Al_2O_3 through the incorporation of Cu^{2+} into the γ-Al_2O_3 framework under varying thermal aging conditions. It was observed that the coordination state of Cu on the γ-Al_2O_3 surface could be manipulated by controlling the O_2 concentration during thermal aging. At high temperatures exceeding 900 °C under low O_2 concentration, Cu_2O dominated due to the thermal decomposition of CuO, fostering the formation of a solid solution between Cu_2O and γ-Al_2O_3. This induced the occupation of the octahedral sites by monovalent Cu^+ (O_h-Cu^+). Conversely, under high O_2 concentrations (50 and 100%), CuO was stabilized, impeding its decomposition into Cu_2O. This led to a solid solution formation between CuO and γ-Al_2O_3, resulting in the occupation of tetrahedral sites by divalent Cu^{2+} (T_d-Cu^{2+}). Additionally, at high temperatures under 100% O_2 concentration, thermal aging inhibited both material crystallization and the phase transition from γ-Al_2O_3 to α-Al_2O_3, favoring the creation of pseudospinel $CuAl_2O_4$. This compound predominantly exhibited a tetrahedrally coordinated surface Cu (T_d-Cu) and a high specific surface area.

Successful preparation of pseudospinel $CuAl_2O_4$ with O_h-Cu involved thermal aging at 900 °C for 25 h in the absence of O_2, while achieving T_d-Cu required thermal aging at 1000 °C for 25 h under 100% O_2. Kinetic analysis revealed that in the former, the rate-determining step of the CO−NO reaction is NO reduction, while in the latter, it is CO oxidation. This significant difference arises from the relative strength of NO adsorption on O_h-Cu and T_d-Cu, where the lower coordination number of T_d-Cu offers a considerable advantage for NO adsorption compared to O_h-Cu. Consequently, the strong NO adsorption inhibits the adsorption of CO on T_d-Cu, directly

https://doi.org/10.1021/acsomega.3c09704
ACS Omega 2024, 9, 11950−11957

impacting its kinetics. While this may negatively affect the CO−NO reaction, it positively influences NO reduction in the three-way catalytic reaction. This material, characterized by a high T_d-Cu ratio, emerges as a promising candidate to replace conventional PGM catalysts, showcasing efficient deNO_x capabilities alongside high thermal stability.

■ ASSOCIATED CONTENT

Supporting Information

The Supporting Information is available free of charge at https://pubs.acs.org/doi/10.1021/acsomega.3c09704.

Data related to CO-TPR, change in specific surface area of Cu on Cu/Al_2O_3 after thermal aging under different O_2 concentrations, XRD patterns, catalytic activity, and change in the DRIFT spectra of CO (PDF)

■ AUTHOR INFORMATION

Corresponding Authors

Aoi Okuda − *Division of Frontier Engineering, Graduate School of Natural Science and Technology, Kanazawa University, Kanazawa 920-1192, Japan*; Email: a5630@stu.kanazawa-u.ac.jp

Hiroshi Yoshida − *Faculty of Frontier Engineering, Institute of Science and Engineering, Kanazawa University, Kanazawa 920-1192, Japan*; orcid.org/0000-0001-9570-477X; Phone: +81-76-264-6260; Email: h-yoshida@se.kanazawa-u.ac.jp

Authors

Taniyuki Furuyama − *Nanomaterials Research Institute, Kanazawa University, Kanazawa 920-1192, Japan*; orcid.org/0000-0002-5435-1581

Toshiaki Sakai − *Engineering and Technology Department, Kanazawa University, Kanazawa 920-1192, Japan*

Masato Machida − *Division of Materials Science and Chemistry, Faculty of Advanced Science and Technology, Kumamoto University, Kumamoto 860-8555, Japan*; orcid.org/0000-0002-6207-7914

Complete contact information is available at: https://pubs.acs.org/10.1021/acsomega.3c09704

Notes

The authors declare no competing financial interest.

■ ACKNOWLEDGMENTS

This study was supported, in part, by a Grant-in-Aid from the Japan Society for the Promotion of Science (grant no. 19H02518) and the Iketani Science and Technology Foundation (0351053-A).

■ REFERENCES

(1) Kašpar, J.; Fornasiero, P.; Hickey, N. Automotive Catalytic Converters: Current Status and Some Perspectives. *Catal. Today* **2003**, *77* (4), 419−449.

(2) Twigg, M. V. Progress and Future Challenges in Controlling Automotive Exhaust Gas Emissions. *Appl. Catal., B* **2007**, *70* (1−4), 2−15.

(3) Beale, A. M.; Gao, F.; Lezcano-Gonzalez, I.; Peden, C. H. F.; Szanyi, J. Recent Advances in Automotive Catalysis for NO_x Emission Control by Small-Pore Microporous Materials. *Chem. Soc. Rev.* **2015**, *44* (20), 7371−7405.

(4) Wu, J.; O'Neill, A. E.; Li, C. H.; Jinschek, J. R.; Cavataio, G. Superior TWC Activity of Rh Supported on Pyrochlore-Phase Ceria Zirconia. *Appl. Catal., B* **2021**, *280*, 119450.

(5) Li, Y. J.; Low, K. B.; Sundermann, A.; Zhu, H. Y.; Betancourt, L. E.; Kang, C. S.; Johnson, S.; Xie, S. H.; Liu, F. D. Understanding the Nature of Pt-Rh Synergy for Three-Way Conversion Catalysis. *Appl. Catal., B* **2023**, *334*, 122821.

(6) Glisenti, A.; Pacella, M.; Guiotto, M.; Natile, M. M.; Canu, P. Largely Cu-Doped $LaCo_{1-x}Cu_xO_3$ Perovskites for TWC: Toward New PGM-Free Catalysts. *Appl. Catal., B* **2016**, *180*, 94−105.

(7) Perin, G.; Fabro, J.; Guiotto, M.; Xin, Q.; Natile, M. M.; Cool, P.; Canu, P.; Glisenti, A. $Cu@LaNiO_3$ Based Nanocomposites in TWC Applications. *Appl. Catal., B* **2017**, *209*, 214−227.

(8) Schön, A.; Dacquin, J.-P.; Granger, P.; Dujardin, C. Non Stoichiometric $La_{1-y}FeO_3$ Perovskite-Based Catalysts as Alternative to Commercial Three-Way-Catalysts?—Impact of Cu and Rh Doping. *Appl. Catal., B* **2018**, *223*, 167−176.

(9) Pacella, M.; Garbujo, A.; Fabro, J.; Guiotto, M.; Xin, Q.; Natile, M. M.; Canu, P.; Cool, P.; Glisenti, A. PGM-Free $CuO/LaCoO_3$ Nanocomposites: New Opportunities for TWC Application. *Appl. Catal., B* **2018**, *227*, 446−458.

(10) Ueda, K.; Tsuji, M.; Ohyama, J.; Satsuma, A. Tandem Base-Metal Oxide Catalyst: Superior NO Reduction Performance to the Rh Catalyst in NO-C_3H_6-CO-O_2. *ACS Catal.* **2019**, *9*, 2866−2869.

(11) Hu, Y. H.; Dong, L.; Shen, M. M.; Liu, D.; Wang, J.; Ding, W. P.; Chen, Y. Influence of supports on the activities of copper oxide species in the low-temperature NO+CO reaction. *Appl. Catal., B* **2001**, *31* (1), 61−69.

(12) Ma, L.; Luo, M.-F.; Chen, S.-Y. Redox Behavior and Catalytic Properties of $CuO/Ce0.8Zr_{0.2}O_2$ Catalysts. *Appl. Catal., A* **2003**, *242* (1), 151−159.

(13) Martínez-Arias, A.; Hungría, A. B.; Iglesias-Juez, A.; Fernández-García, M.; Anderson, J. A.; Conesa, J. C.; Munuera, G.; Soria, J. Redox and Catalytic Properties of CuO/CeO_2 under CO+O_2+NO: Promoting Effect of NO on CO Oxidation. *Catal. Today* **2012**, *180* (1), 81−87.

(14) Yao, X.; Yu, Q.; Ji, Z.; Lv, Y.; Cao, Y.; Tang, C.; Gao, F.; Dong, L.; Chen, Y. A Comparative Study of Different Doped Metal Cations on the Reduction, Adsorption and Activity of $CuO/Ce_{0.67}M_{0.33}O_2$ (M = Zr^{4+}, Sn^{4+}, Ti^{4+}) Catalysts for NO+CO Reaction. *Appl. Catal., B* **2013**, *130*−*131*, 293−304.

(15) Tan, W.; Xie, S. H.; Wang, X.; Xu, J. T.; Yan, Y.; Ma, K. L.; Cai, Y. D.; Ye, K. L.; Gao, F.; Dong, L.; Liu, F. D. Determination of Intrinsic Active Sites on $CuO-CeO_2-Al_2O_3$ Catalysts for CO Oxidation and NO Reduction by CO: Differences and Connections. *ACS Catal.* **2022**, *12* (20), 12643−12657.

(16) Yoshida, H.; Okabe, Y.; Yamashita, N.; Hinokuma, S.; Machida, M. Catalytic CO-NO Reaction Over Cr-Cu Embedded CeO_2 Surface Structure. *Catal. Today* **2017**, *281*, 590−595.

(17) Yoshida, H.; Okabe, Y.; Misumi, S.; Oyama, H.; Tokusada, K.; Hinokuma, S.; Machida, M. Structures and Catalytic Properties of Cr-Cu Embedded CeO_2 Surfaces With Different Cr/Cu Ratios. *J. Phys. Chem. C* **2016**, *120* (47), 26852−26863.

(18) Yoshida, H.; Hirakawa, T.; Oyama, H.; Nakashima, R.; Hinokuma, S.; Machida, M. Effect of Thermal Aging on Local Structure and Three-Way Catalysis of Cu/Al_2O_3. *J. Phys. Chem. C* **2019**, *123* (16), 10469−10476.

(19) Wang, Y.; Zhu, A.; Zhang, Y.; Au, C. T.; Yang, X.; Shi, C. Catalytic Reduction of NO by CO Over NiO/CeO_2 Catalyst in Stoichiometric NO/CO and NO/CO/O_2 Reaction. *Appl. Catal., B* **2008**, *81* (1−2), 141−149.

(20) Cheng, X.; Zhu, A.; Zhang, Y.; Wang, Y.; Au, C. T.; Shi, C. A Combined DRIFTS and MS Study on Reaction Mechanism Of NO Reduction by CO Over NiO/CeO_2 Catalyst. *Appl. Catal., B* **2009**, *90* (3−4), 395−404.

(21) Yoshida, H.; Kawakami, Y.; Tokuzumi, W.; Shimokawa, Y.; Hirakawa, T.; Ohyama, J.; Machida, M. Low-Temperature NO Reduction Over Fe-Ni Alloy Nanoparticles Using Synergistic Effects

of Fe and Ni in a Catalytic NO-CO-C_3H_6-O_2 reaction. *Bull. Chem. Soc. Jpn.* **2020**, *93* (9), 1050−1055.
(22) Liotta, L. F.; Pantaleo, G.; Di Carlo, G.; Marcì, G.; Deganello, G. Structural and Morphological Investigation of a Cobalt Catalyst Supported On Alumina-Baria: Effects of Redox Treatments on the Activity in the NO Reduction by CO. *Appl. Catal., B* **2004**, *52* (1), 1−10.
(23) Praliaud, H.; Mikhailenko, S.; Chajar, Z.; Primet, M. Surface and Bulk Properties of Cu-ZSM-5 and Cu/Al_2O_3 Solids During Redox Treatments. Correlation With the Selective Reduction of Nitric Oxide by Hydrocarbons. *Appl. Catal., B* **1998**, *16* (4), 359−374.
(24) Ueda, K.; Tsuji, M.; Ohyama, J.; Satsuma, A. Active Coordination Sites of Co Spinel Oxides for NO Reduction by CO. *Catal. Today* **2023**, *411*−*412*, 113816.
(25) Papavasiliou, A.; Tsetsekou, A.; Matsouka, V.; Konsolakis, M.; Yentekakis, I. V.; Boukos, N. Synergistic Structural and Surface Promotion of Monometallic (Pt) TWCs: Effectiveness and Thermal Aging Tolerance. *Appl. Catal., B* **2011**, *106* (1−2), 228−241.
(26) Heo, I.; Yoon, D. Y.; Cho, B. K.; Nam, I. S.; Choung, J. W.; Yoo, S. Activity and Thermal Stability of Rh-Based Catalytic System for an Advanced Modern TWC. *Appl. Catal., B* **2012**, *121*−*122*, 75−87.
(27) Yoshida, H.; Oyama, H.; Shiomori, R.; Hirakawa, T.; Ohyama, J.; Machida, M. Enhanced Catalytic NO Reduction in NO-CO-C_3H_6-O_2 Reaction Using Pseudo-Spinel (NiCu)Al_2O_4 Supported on γ-Al_2O_3. *ACS Catal.* **2021**, *11* (12), 7302−7309.
(28) Jiang, X.; Fan, J.; Xiang, S. Y.; Mou, J. L.; Yao, P.; Jiao, Y.; Wang, J. L.; Chen, Y. Q. Superior Catalytic Activity and High Thermal Durability of $MgAl_2O_4$ Modified Pt/$Ce_{0.5}Zr_{0.5}O_2$ TWC. *Appl. Surf. Sci.* **2022**, *578*, 151915.
(29) Amano, F.; Suzuki, S.; Yamamoto, T.; Tanaka, T. One-Electron Reducibility of Isolated Copper Oxide on Alumina for Selective NO-CO Reaction. *Appl. Catal., B* **2006**, *64* (3−4), 282−289.
(30) Yamamoto, T.; Tanaka, T.; Kuma, R.; Suzuki, S.; Amano, F.; Shimooka, Y.; Kohno, Y.; Funabiki, T.; Yoshida, S. NO Reduction With CO in the Presence of O_2 Over Al_2O_3-Supported and Cu-Based Catalysts. *Phys. Chem. Chem. Phys.* **2002**, *4* (11), 2449−2458.
(31) Yoshida, H.; Yamashita, N.; Ijichi, S.; Okabe, Y.; Misumi, S.; Hinokuma, S.; Machida, M. A Thermally Stable Cr-Cu Nanostructure Embedded in the CeO_2 Surface as a Substitute for Platinum-Group Metal Catalysts. *ACS Catal.* **2015**, *5* (11), 6738−6747.
(32) Koizumi, K.; Yoshida, H.; Boero, M.; Tamai, K.; Hosokawa, S.; Tanaka, T.; Nobusada, K.; Machida, M. A Detailed Insight Into the Catalytic Reduction of NO Operated by Cr-Cu Nanostructures Embedded in a CeO_2 Surface. *Phys. Chem. Chem. Phys.* **2018**, *20* (40), 25592−25601.
(33) Obeid, M. M.; Mogulkoc, Y.; Edrees, S. J.; Ciftci, Y. O.; Shukur, M. M.; Al-Marzooqee, M. H. Analysis of the Structural, Electronic, Elastic and Thermodynamic Properties of $CuAl_2X_4$ (X = O, S) Spinel Structure. *Mater. Res. Bull.* **2018**, *108*, 255−265.
(34) Prins, R. Location of the Spinel Vacancies in γ-Al_2O_3. *Angew. Chem., Int. Ed.* **2019**, *58* (43), 15548−15552.
(35) Areán, C. O.; Vinuela, J. S. D. Structural Study of Copper Nickel Aluminate ($Cu_xNi_{1-x}Al_2O_4$) Spinels. *J. Solid State Chem.* **1985**, *60* (1), 1−5.
(36) Kim, T. W.; Song, M. W.; Koh, H. L.; Kim, K. L. Surface Properties and Reactivity of Cu/γ-Al_2O_3 Catalysts for NO Reduction by C_3H_6: Influences of Calcination Temperatures and Additives. *Appl. Catal., A* **2001**, *210* (1−2), 35−44.
(37) Yahiro, H.; Nakaya, K.; Yamamoto, T.; Saiki, K.; Yamaura, H. Effect of Calcination Temperature on the Catalytic Activity of Copper Supported on γ-Alumina for the Water-Gas-Shift Reaction. *Catal. Commun.* **2006**, *7* (4), 228−231.
(38) Xu, Y.; Lin, Z. Y.; Zheng, Y. Y.; Dacquin, J. P.; Royer, S.; Zhang, H. Mechanism and Kinetics of Catalytic Ozonation for Elimination of Organic Compounds With Spinel-Type $CuAl_2O_4$ and Its Precursor. *Sci. Total Environ.* **2019**, *651*, 2585−2596.
(39) Shimizu, K.; Kawabata, H.; Maeshima, H.; Satsuma, A.; Hattori, T. Intermediates in the Selective Reduction of NO by Propene Over Cu-Al_2O_3 Catalysts: Transient In-Situ FTIR Study. *J. Phys. Chem. B* **2000**, *104* (13), 2885−2893.
(40) Hong, Z.; Jin, Y. X.; Wang, S. Y.; Gao, Z. H.; Huang, W. Enhanced Catalytic Stability of Non-Stoichiometric Cu-Al Spinel Catalysts for Dimethyl Ether Synthesis From Syngas: Effect of Coordination Structure. *Fuel Process. Technol.* **2023**, *247*, 107772.
(41) Chen, L.; Horiuchi, T.; Osaki, T.; Mori, T. Catalytic Selective Reduction of NO with Propylene over Cu-Al_2O_3 Catalysts: Influence of Catalyst Preparation Method. *Appl. Catal., B* **1999**, *23*, 259−269.
(42) Shimizu, K.; Maeshima, H.; Yoshida, H.; Satsuma, A.; Hattori, T. Spectroscopic Characterisation of Cu-Al_2O_3 Catalysts for Selective Catalytic Reduction of NO with Propene. *Phys. Chem. Chem. Phys.* **2000**, *2*, 2435−2439.
(43) Padley, M. B.; Rochester, C. H.; Hutchings, G. J.; King, F. FTIR Spectroscopic Study of Thiophene, SO_2, and CO Adsorption on Cu/Al_2O_3 Catalysts. *J. Catal.* **1994**, *148*, 438−452.
(44) Li, D.; Yu, Q.; Li, S. S.; Wan, H. Q.; Liu, L. J.; Qi, L.; Liu, B.; Gao, F.; Dong, L.; Chen, Y. The Remarkable Enhancement of CO-Pretreated CuO-Mn_2O_3/γ-Al_2O_3 Supported Catalyst for the Reduction of NO with CO: The Formation of Surface Synergetic Oxygen Vacancy. *Chem. - Eur. J.* **2011**, *17*, 5668−5679.
(45) Venkov, T.; Dimitrov, M.; Hadjiivanov, K. FTIR Spectroscopic Study of the Nature and Reactivity of NO_x Compounds Formed on Cu/Al_2O_3 after Coadsorption of NO and O_2. *J. Mol. Catal. A: Chem.* **2006**, *243*, 8−16.
(46) Ramprasad, R.; Hass, K. C.; Schneider, W. F.; Adams, J. B. Cu-Dinitrosyl Species in Zeolites: A Density Functional Molecular Cluster Study. *J. Phys. Chem. B* **1997**, *101* (35), 6903−6913.
(47) Zhanpeisov, N. U.; Matsuoka, M.; Mishima, H.; Yamashita, H.; Anpo, M. Interaction of NO molecules with a copper-containing zeolite. *J. Mol. Struct.: THEOCHEM* **1998**, *454* (2−3), 201−207.

https://doi.org/10.1021/acsomega.3c09704
ACS Omega 2024, 9, 11950−11957